LA-UR-22-30105

Approved for public release; distribution is unlimited.

Title:	Scalable Experimental Bounds for Dicke and GHZ States Fidelities
Author(s):	Aktar, Shamminuj Baertschi, Andreas Badawy, Abdel-Hameed Eidenbenz, Stephan Johannes
Intended for:	20th ACM International Conference on Computing Frontiers CF'23, 2023-05-09/2023-05-11 (Bologna, Italy) arXiv
Issued:	2023-10-09 (rev.1)

Scalable Experimental Bounds for Dicke and GHZ States Fidelities

Shamminuj Aktar
Klipsch School of Electrical and Computer Engineering
New Mexico State University
Las Cruces, NM, 88001, USA
saktar@nmsu.edu

Andreas Bärtschi
CCS-3 Information Sciences
Los Alamos National Laboratory
Los Alamos, NM, 87544, USA
baertschi@lanl.gov

Abdel-Hameed A. Badawy
Klipsch School of Electrical and Computer Engineering
New Mexico State University
Las Cruces, NM, 88001, USA
badawy@nmsu.edu

Stephan Eidenbenz
CCS-3 Information Sciences
Los Alamos National Laboratory
Los Alamos, NM, 87544, USA
eidenben@lanl.gov

ABSTRACT

Estimating the state preparation fidelity of highly entangled states on noisy intermediate-scale quantum (NISQ) devices is an important task for benchmarking and application considerations. Unfortunately, exact fidelity measurements quickly become prohibitively expensive, as they scale exponentially as $O(3^N)$ for N-qubit states, using full state tomography with measurements in all Pauli bases combinations. However, Somma *et al.* [20] established that the complexity could be drastically reduced when looking at *fidelity lower bounds* for states that exhibit symmetries, such as Dicke States and GHZ States. For larger states, these bounds still need to be tight enough to provide reasonable estimations on NISQ devices.

For the first time and more than 15 years after the theoretical introduction, we report meaningful lower bounds for the state preparation fidelity of all Dicke States up to $N = 10$, and all GHZ states up to $N = 20$ on Quantinuum H1 ion-trap systems using efficient implementations of recently proposed scalable circuits for these states. Our achieved lower bounds match or exceed previously reported exact fidelities on superconducting systems for much smaller states. This work provides a path forward to benchmarking entanglement as NISQ devices improve in size and quality.

KEYWORDS

Fidelity, Entangled States, State Tomography, Quantinuum

1 INTRODUCTION

Any advantage that quantum computing may have over classic computing usually relies on the principle of superposition, informally defined as being simultaneously in multiple computational basis states. Quantum states that are in a superposition such that individual parts cannot be described independently of the state of others are called entangled states. Superposition and entanglement are essential prerequisites for the successful execution of additional gate operations per the overall structure of the quantum algorithm executed to lead to a desired quantum end state ultimately. Thus, proving that a NISQ device produces entangled states is necessary for any quantum computing success. Such low-level testing of quantum mechanical properties is necessary on quantum devices because environmental noise quickly modifies or partially destroys a pure quantum state (as it would be theoretically prepared); this noise process, usually called decoherence, turns the actual state in a computing device into a so-called mixed state, which is a probabilistic mixture of our target pure quantum state and other pure states. The fidelity of a (mixed) quantum state measures to what extent the intended target (pure) quantum state has been realized. Fidelity is defined as '1' if we measure a correct pure quantum state and close to zero, *i.e.*, $1/2^N$ for a maximally mixed N-qubit quantum state that consists purely of noise.

Let us use the state $\frac{1}{\sqrt{2}}(|00\rangle + |11\rangle)$, *i.e.*, the Bell state as the prototypical entangled state to illustrate the concept of fidelity. From a classical vantage point, it may appear tempting to test whether a NISQ device has actually produced a Bell state as follows: We execute a large number of runs of the generating circuit, each with measurement at the end, and count how often we measure 00, 01, 10, and 11. If we measure 00 and 11 about 50 percent of the time each, we declare that the devices actually produce the Bell state. However, this logic is flawed because any classical device that simply returns 00 and 11 with probability 0.5 would have also passed such a test. Such a cheat device would be useless and unable to properly execute additional gate operations that propagate the quantum state and its entanglement properly to execute any full quantum algorithm. The appropriate way to test entanglement is to calculate the fidelity measure (will formally define later), which measures the outcome in all possible combination bases of X, Y, and Z axes. This requires 3^N tests for N-qubit states and is called full-state tomography. A fidelity measure of '1' indicates a perfect quantum state (with entanglement), whereas a value of '0' indicates a state without entanglement.

Showing that entanglement exists on NISQ devices across more than '10' qubits is computationally prohibitive due to the exponential number of tests. Nevertheless, it remains vital to demonstrate that the device leverages quantum mechanical principles.

A solution to this dilemma is to approximate or compute bounds on the fidelity measure that require fewer runs to calculate. Somma *et al.* [20] discovered such bounds for certain symmetric entangled states based on angular momentum operators.

This research was supported by a Laboratory Directed Research and Development program of Los Alamos National Laboratory under project number 20220656ER. This research used resources from the Oak Ridge Leadership Computing Facility, which is a DOE Office of Science User Facility supported under Contract DE-AC05-00OR22725. Ms. Aktar is supported by a College of Engineering at New Mexico State University Fellowship. This work has been approved for public release, LA-UR-22-30105.

In this paper, we adopt and modify these generic bounds for the Dicke and GHZ states – two well-known classes of entangled states. Dicke states are equal amplitude superpositions of all computational states of the same Hamming weight (*i.e.*, number of ones). GHZ states are Bell states that are generalized to larger qubit counts. Both Dicke & GHZ states are studied extensively because of their quantum mechanical properties and their use in various domains.

Through a series of NISQ experiments, we show that the bound from [20] has become useful in practice to provide evidence for entanglement across up to '20' qubits without resorting to exponentially expensive full-state tomography. This is a testament to advances in state preparation algorithms and NISQ hardware improvements. Figure 1 shows that the original bounds are not useful for NISQ devices from just two years ago for Dicke states on as few as '5' qubits as they give negative values; they become slightly positive with our modifications without providing strong evidence of entanglement; however, newer devices (Quantinuum) produce results good enough for these bounds to become meaningful lower bounds for fidelity. The original and our modified fidelity bounds require only three different measurement runs, thus making fidelity-based entanglement verification easy on NISQ devices, even at high qubit counts.

The contributions of the paper are as follows:

- We propose a divide-and-conquer based efficient Dicke state preparation circuits with $O(N)$ circuit depth and $O(KN)$ gate count with low constant factors.
- We utilize and improve the lower bounds on the quantum fidelity from theory [20] using only three measurement settings for Dicke states and only two for GHZ states.
- We demonstrate, using large-scale experiments on Dicke and GHZ state preparation on Quantinuum's H1 ion-trap quantum device, the usefulness of the bounds for the first time on real quantum hardware.
- We report meaningful lower bound for all Dicke States up to '10' qubits and all GHZ states up to '20' qubits using efficient circuit implementations.
- We give state preparation fidelities that match or exceed exact fidelity records. For example, we give state preparation fidelity lower bounds of (i) 0.46 for the '10' qubit Dicke State $|D_5^{10}\rangle$ and (ii) 0.73 for the '20' qubit GHZ State $|G_{20}\rangle$. These match or exceed exact fidelity records recently achieved on IBM's superconducting systems for much smaller states $|D_3^6\rangle$ [3], and $|G_5\rangle$ [7], respectively.

The rest of the paper is organized as follows: Section 2 summarizes the related works on fidelity estimation. Section 3 includes our experimental methodology. Sections 4 & 5 go over the state preparation, lower bound estimation, and experimental results for Dicke and GHZ states. Finally, Section 6 concludes the paper.

2 RELATED WORK

We use the *quantum fidelity* $\mathcal{F}$ as a similarity measure between a prepared mixed state ρ, expressed as a density matrix, and a target pure quantum state $\rho_\psi = |\psi\rangle\langle\psi|$ [13]:

$$\mathcal{F}(\rho_\psi, \rho) = \left[\mathrm{Tr}\sqrt{\sqrt{\rho}\rho_\psi\sqrt{\rho}}\right]^2 = \mathrm{Tr}(\rho_\psi\rho) = \langle\psi|\,\rho\,|\psi\rangle \qquad (1)$$

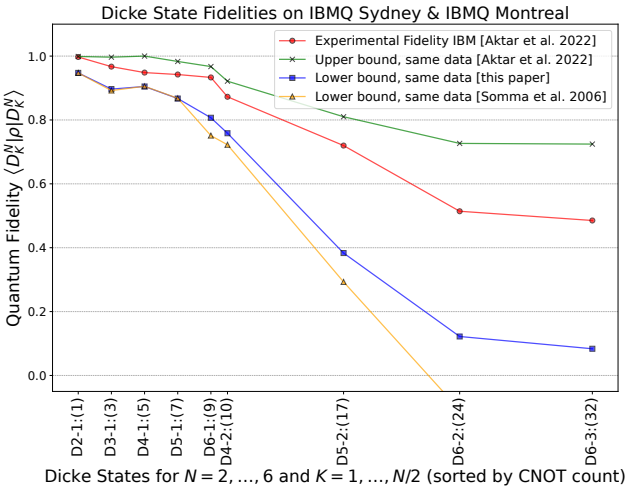

Figure 1: Experimental fidelities of Dicke states $|D_K^N\rangle$ (by circuit complexity) on IBMQ devices based on full state tomography data [3, Aktar *et al.*]: *(red)* Exact fidelity computed from all 3^N tomography measurement settings, *(green)* Upper bound computed only from the Z-basis measurement data. *(blue)* We compute fidelity lower bounds from experimental X-, Y-, and Z-basis measurement setting subsets of their data, slightly improving on direct application of existing lower bound techniques [20, Somma *et al.*] *(orange).*

where $\sqrt{\rho}$ denotes the unique positive semi-definite square root of ρ such that $\sqrt{\rho}\sqrt{\rho} = \sqrt{\rho}^\dagger\sqrt{\rho} = \rho$, and where the first equality would also hold for a mixed state ρ_ψ.

In this paper, we consider pure target states, notably Dicke states $|D_K^N\rangle$ and GHZ states $|G_N\rangle$. We remark that quantum fidelity is sometimes also defined as $\mathcal{F}' = \sqrt{\mathcal{F}}$ [18, 20]. In a straightforward way, the fidelity of a prepared N-qubit state can be computed by sampling ρ in 3^N different Pauli basis (N-fold tensor products of Pauli operators σ_x,σ_y and σ_z) to reconstruct its density matrix; hence we can compute the fidelity with the target state.

Suppose we want to *upper bound* the quantum fidelity. In that case, we can consider the *measurement success probability*, *i.e.*, the overall probability of sampling non-zero amplitude states when measuring in the computational Z-basis:

$$MSP(\rho_\psi, \rho) := \sum\nolimits_{x\in\{0,1\}^n,\ \langle x|\rho_\psi|x\rangle\neq 0} \langle x|\,\rho\,|x\rangle \qquad (2)$$

Using a double application of the Cauchy-Schwarz inequality, one gets $\mathcal{F}(\rho_\psi, \rho) \leq MSP(\rho_\psi, \rho)$ [3].

Several works have shown that it is possible to estimate a *lower bound* on the quantum fidelity using only a few measurement settings, avoiding full-state tomography. Earlier works [11, 20] focused on certain states with unique symmetry that require only a small random subset of Pauli operators to estimate fidelity. Somma *et al.* [20] proposed expressions for estimating quantum fidelity for highly symmetric classes of multi-qubit state preparation, *i.e.*, rotational invariant states, stabilizer states, and generalized coherent

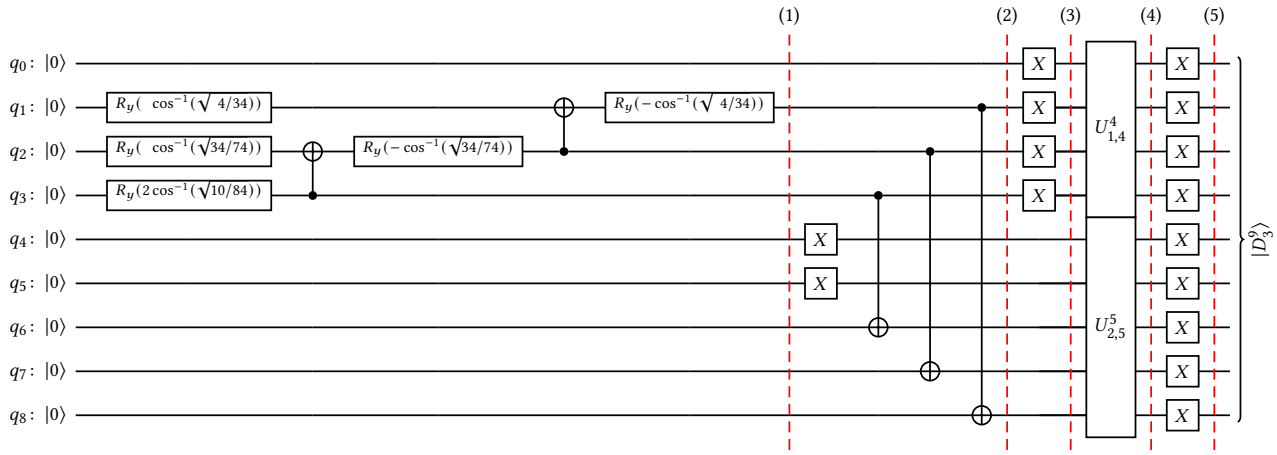

Figure 2: Divide-and-conquer Dicke state $|D^9_3\rangle$ preparation allowing parallelizable Dicke state unitaries on 4 and 5 qubits: *(1)* We prepare a correctly weighted superposition of input Hamming weights $0 \le \ell \le 3$ on the first register. The used R_y-rotations contain arguments with numerators (denominators) derived from (suffix-sums) of terms of the form $\binom{5}{3-\ell}\binom{4}{\ell}$, the number of distributions of ℓ & $3-\ell$ Ones across 4 & 5 qubits. *(2&3)* The first register is correctly entangled with the second register, and bit-flipping X-gates are applied to reduce the number of CNOTs in the following. *(4&5)* Parallel Dicke state unitaries $U^4_{1,4}$ and $U^5_{2,5}$ prepare the Dicke state $|D^9_6\rangle$, followed by bit-flipping X-gates to get $|D^9_3\rangle$.

states. To estimate the lower fidelity bound, they only used the measurements related to the symmetry operators of the density matrix. Guhne *et al.* [11] derived fidelity estimation for *GHZ* and *W* states using $2N-1$ measurements. Flammia *et al.* [9] had a generalized approach where they showed estimation techniques for all possible state preparation by measuring fewer Pauli operators close to the desired state and of greater importance. Mentioning the scalability issue in generalized N qubit state fidelity estimation, Elben *et al.* [8] showed how randomized measurement could enable fidelity estimation by comparing two states. Recently, Zhang *et al.* [25] proposed a machine learning (ML) approach for direct fidelity estimation as a classification problem using a constant number of expectations.

Additionally, quantum state verification (also known as the non-tomographic method) uses advanced statistical approaches to verify whether the output of some device is the target state. Previous works on quantum state verification techniques validate specific state preparation such as Dicke states [16], GHZ states [15], Hypergraph states [26], Pure states [14, 22, 23, 27], *etc.* There are also some generalized approaches for state verification [12, 19, 21, 24, 28, 29].

3 METHODOLOGY

In this work, we ran the experiments on both the hardware and emulator devices of Quantinuum H-systems [2] using the Quantinuum Python API. Running jobs on the Quantinuum backend requires H-System Quantum Credits (HQC) that are linear with both the number of shots per circuit and the number of CNOTs in the circuit. In general, the total cost scales with the product of the number of shots and CNOT counts. Our initial goal was to determine the number of experiments and the number of shots for different state preparation permissible within the HQCs allocated to us. As the Quantinuum machines are available through a calendar month and HQCs are allocated monthly, we target to complete experiments throughout several months with available hardware credits.

First, we ran the experiments on the Quantinuum H1-2E emulator to estimate the confidence interval sizes we can expect from the quantum hardware. To see the effect of the number of circuit executions, we compute the cumulative bounds for fidelity and measure success probability. Similarly, we compute a two-sided 68% confidence interval below and above the mean of the distribution to check the stability of the bounds with the increasing number of shots. Analyzing the results of emulator experiments, we get an approximation of a meaningful number of experiments that can be performed on quantum hardware for various states. We limit Dicke state preparation up to $N = 10$ as Dicke States starting at $N = 11$ become prohibitively expensive computationally. For GHZ states, we went up to $N = 20$ as we ran the experiment on a 20-qubit H1-1 device. Additionally, we observe roughly equal confidence interval widths for the bounds across the experiments. Next, we execute the experiments of different state preparation on Quantinuum hardware backends, depending on their availability. Dicke state circuits were executed in the '12' qubit H1-2 processor, while GHZ state circuits were executed in the '20' qubit H1-1 processor. For all experiments, we generate the circuits using IBM Qiskit [1] and directly submit the QASM [6] code using the Python API. To execute the circuits in the same time span, we submit the jobs in batch mode; thus, we wait for the queue time once. However, the Quantinuum queue only allows 500 HQC execution in a single batch. Thus, we executed sub-experiments over a couple of months.

4 FIDELITY LOWER BOUNDS FOR DICKE STATES

We provide experimental lower bound estimations on the state preparation fidelity of Dicke states $|D^N_K\rangle$ (up to $N = 10$). We first

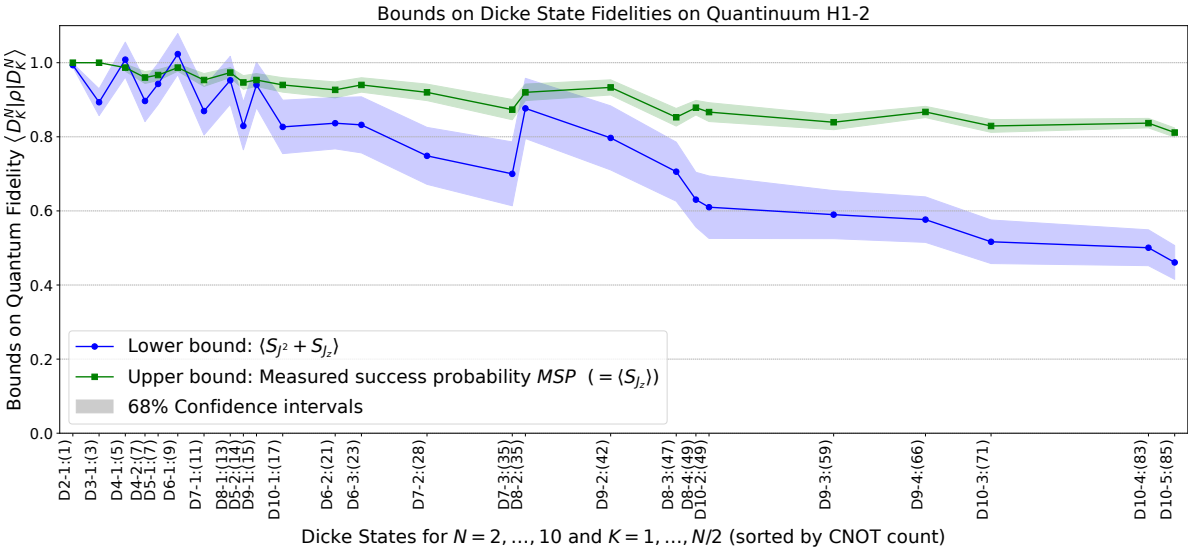

Figure 3: Upper and lower bounds on the quantum fidelity $\langle D_K^N|\,\rho\,|D_K^N\rangle$ for Dicke States $|D_K^N\rangle$ on Quantinuum H1-2, including 68% confidence intervals. Dicke states are sorted along the x-axis according to the number of CNOTs in their preparation circuits. The bump in fidelity for Dicke states $|D_1^8\rangle$–$|D_4^8\rangle$ and $|D_1^9\rangle$–$|D_2^9\rangle$ may be due to these experiments taking place right after a recalibration downtime of the QPU.

discuss the circuit preparation strategies, then provide lower bound expressions for estimating quantum fidelity, and present experimental results for fidelity estimation in Quantinuum's H1-2 device.

4.1 State Preparation

A Dicke state $|D_K^N\rangle$ is the equal weight superposition of all $\binom{N}{K}$ N-qubit basis states x with K Ones and $N-K$ Zeroes, *i.e.*, with Hamming weight $\mathrm{wt}(x)=K$:

$$|D_K^N\rangle = \binom{N}{K}^{-1/2} \sum_{x\in\{0,1\}^N,\ \mathrm{wt}(x)=K} |x\rangle. \tag{3}$$

We optimize and generalize existing work on Dicke state preparation by defining Dicke state unitaries $U_{k,K}^N$, which prepare Dicke states $|D_\ell^N\rangle$ upon any input of a unary encoded Hamming weight $k\le\ell\le K$:

$$U_{k,K}^N\colon \left|0^{N-\ell}1^\ell\right\rangle \mapsto |D_\ell^N\rangle \qquad \forall k\le\ell\le K. \tag{4}$$

Dicke state unitaries were first defined for $k:=0$ [4], and there exists a linear-depth circuit construction for $k:=0$, $K:=N$ with $5\binom{N-1}{2}+2(N-1)$ two-qubit CNOT gates between neighboring qubits in a 1D Linear Nearest Neighbor (LNN) connectivity only [3]. We start from this construction and further reduce the CNOT count by $3\binom{N-K-1}{2}$ and $5\binom{k}{2}$ using ideas for upper [4] and lower [17] bounds on the Hamming weight ℓ, respectively. This effectively generalizes and also improves all of the former constructions by constant factors while preserving LNN connectivity.

To prepare a fixed-K Dicke state $|D_K^N\rangle$, we further parallelize our construction using the divide-and-conquer strategy in [3, 5]: The main idea is to split the Hamming weight K across qubit sets of size $N_1=\lfloor\frac{N}{2}\rfloor$ and $N_2=\lceil\frac{N}{2}\rceil$ using $2K-1$ CNOT gates on an all-to-all connectivity before applying the Dicke state unitaries $U_{0,K}^{N1}$ and $U_{0,K}^{N2}$ in parallel. Additional gains can be made by implementing these unitaries with layers of bit-flipping Pauli-X gates, $U_{0,K}^{N_i}=X^{\otimes N_i}\cdot U_{N_i-K,N_i}^{N_i}\cdot X^{\otimes N_i}$, resulting in the circuit structure shown in Figure 2, which prepares $|D_3^9\rangle$ with the following steps:

$$\begin{aligned}
|0^5\rangle|0^4\rangle &\overset{(1)}{\longmapsto} \tbinom{9}{3}^{-1/2}\sum_{\ell=0}^{3}\sqrt{\tbinom{5}{3-\ell}\tbinom{4}{\ell}}\,|00000\rangle\,|1^\ell 0^{3-\ell}0\rangle\\
&\overset{(2)}{\longmapsto} \tbinom{9}{3}^{-1/2}\sum\sqrt{\tbinom{5}{3-\ell}\tbinom{4}{\ell}}\,|0^{3-\ell}1^\ell 11\rangle\,|1^\ell 0^{3-\ell}0\rangle\\
&\overset{(3)}{\longmapsto} \tbinom{9}{3}^{-1/2}\sum\sqrt{\tbinom{5}{3-\ell}\tbinom{4}{\ell}}\,|0^{3-\ell}1^\ell 11\rangle\,|0^\ell 1^{3-\ell}1\rangle\\
&\overset{(4)}{\longmapsto} \tbinom{9}{3}^{-1/2}\sum\sqrt{\tbinom{5}{3-\ell}\tbinom{4}{\ell}}\,|D_{2+\ell}^5\rangle\,|D_{4-\ell}^4\rangle\\
&\overset{(5)}{\longmapsto} \tbinom{9}{3}^{-1/2}\sum\sqrt{\tbinom{5}{3-\ell}\tbinom{4}{\ell}}\,|D_{3-\ell}^5\rangle\,|D_\ell^4\rangle = |D_3^9\rangle\,.
\end{aligned}$$

Note that to prepare the Dicke state $|D_6^9\rangle$, we can simply omit the last layer of Pauli-X gates. Thus, in our experiments we only prepare Dicke states $|D_K^N\rangle$ up to $K\le\frac{N}{2}$, for which our two-qubit gates amount to $5K(N-K)-3(N+K)+5$ CNOTs, giving linear depth $O(N)$ and total gate count $O(KN)$.

4.2 Lower bounds for fidelity estimation

Following [20], we observe that Dicke States are rotationally invariant and thus are the unique simultaneous eigenstates of the (squared) total angular momentum $J^2=J_x^2+J_y^2+J_z^2$ and its z-component J_z, where $J_\tau=\sigma_\tau^1+\sigma_\tau^2+\ldots+\sigma_\tau^N$ for Pauli operators σ_τ^i, $\tau=x,y,z$, acting on qubit i. This means we can write the Dicke state $|D_K^N\rangle$ as $|j,j_z\rangle$ in terms of its quantum numbers $j=N$ and $j_z=N-2K$ with:

$$J^2\,|j,j_z\rangle = j(j+2)\,|j,j_z\rangle \tag{5}$$

$$J_z\,|j,j_z\rangle = j_z\,|j,j_z\rangle\,. \tag{6}$$

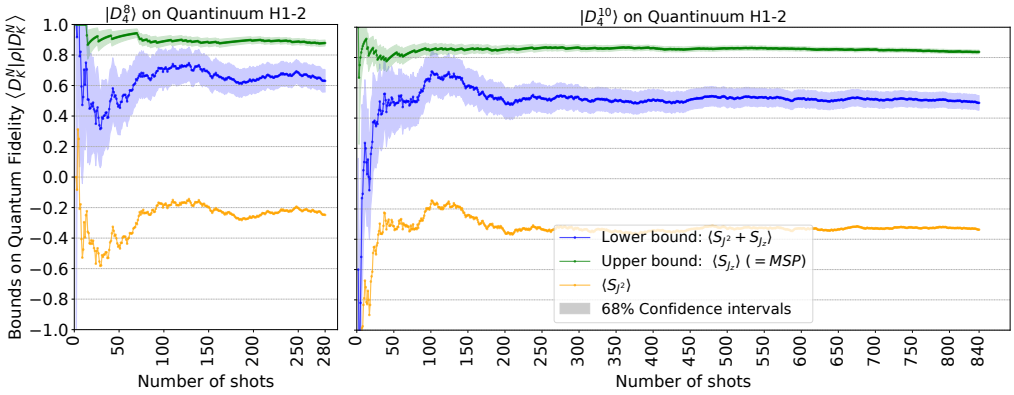

Figure 4: Evolving bounds and confidence intervals on Dicke state fidelity $\langle D_K^N|\,\rho\,|D_K^N\rangle$ for $|D_4^8\rangle$ and $|D_4^{10}\rangle$ on Quantinuum H1-2 with increasing shot count. Experiments were run for 280 and 840 shots for $|D_4^8\rangle$ and $|D_4^{10}\rangle$, respectively, to achieve comparable confidence intervals. Plots are scaled (1:3) accordingly.

In general, the quantum numbers j and j_z satisfy $0 \le j \le N$ and $|j_z| \le j$. The difference between any two eigenvalues is at least 2 (because we use Pauli operators instead of spin-1/2 operators).

Now, we can write a target state $\rho_{j,j_z} := |j, j_z\rangle\langle j, j_z|$ in terms of the operators J^2 and J_z:

$$\rho_{j,j_z} = \prod_{\substack{j_z' \neq j_z \\ -j \le j_z' \le j}} \frac{J_z - j_z'}{j_z - j_z'} \prod_{\substack{j' \neq j \\ 0 \le j' \le N}} \frac{J^2 - j'(j'+2)}{j(j+2) - j'(j'+2)}. \tag{7}$$

We could compute the fidelity $\mathcal{F}(\rho_{j,j_z}, \rho)$ by measuring every Pauli-String appearing when we expand the product, *i.e.*, all correlations between the operators J^2 and J_z in Equation (7). This process requires measurement of an exponentially large number of observables but less than 3^N measurements of performing full-state tomography.

Instead, we turn towards the construction of operators that allow us to compute a lower bound on the fidelity. We will define operators $\mathcal{S}_{J_z}$ and $\mathcal{S}_{J^2}$ inspired by the density operator of Equation (7) such that they satisfy $[\mathcal{S}_{J_z} + \mathcal{S}_{J^2}]\,|j', j_z'\rangle = e_{j',j_z'}\,|j', j_z'\rangle$ with $e_{j',j_z'} = 1$ for the correct Dicke state and $e_{j',j_z'} \le 0$ for $(j', j_z') \neq (j, j_z)$. We define the operator $\mathcal{S}_{J_z}$ as the left-hand product in Equation (7),

$$\mathcal{S}_{J_z} := \prod\nolimits_{j_z' \neq j_z} [(J_z - j_z')/(j_z - j_z')], \tag{8}$$

for which $|j', j_z'\rangle$ has eigenvalue 1 if $j_z' = j_z$ and 0 otherwise.[1] Expanding the product results in Pauli-Strings consisting of identities and σ_z operators only. These commute pairwise, hence we can measure $\mathcal{S}_{J_z}$ in the computational basis and thus in a single measurement setting. In fact, we get the measurement success probability $\mathrm{Tr}\left[\mathcal{S}_{J_z} \cdot \rho\right] = MSP(\rho_{j,j_z}, \rho)$.

The same is not true if we expanded the right-hand product of Equation (7): we would get a large number of non-commuting Pauli-Strings. Instead we use the following definition for $\mathcal{S}_{J^2}$ [20], which is based on the observation that Dicke states have maximum angular momentum, and all other eigenvalues for J^2 deviate by at least $N(N+2) - (N-2)N = 4N$:

$$\mathcal{S}_{J^2} = \tfrac{1}{4N}(J^2 - N(N+2)), \tag{9}$$

for which $|j', j_z'\rangle$ has eigenvalue 0 if $j' = j = N$ and integer eigenvalues ≤ -1 otherwise. Similar to $\mathcal{S}_{J_z}$, we can measure the operator $\mathcal{S}_{J^2}$ by computing $\mathrm{Tr}\left[J_\tau^2 \cdot \rho\right]$ through measurement in the τ-basis, *i.e.*, measuring in the three X-basis, Y-basis and Z-basis settings is enough.

If the sum of the operators $\mathcal{S}_{J_z}$ and $\mathcal{S}_{J^2}$ are applied to a target Dicke state $\rho = |j', j_z'\rangle$, we get eigenvalue 1 for the correct Dicke state and eigenvalues ≤ 0 for all other rotational states. In general, if $|\phi\rangle = \sum_{j',j_z'} c_{j',j_z'}\,|j', j_z'\rangle$ is a pure state, then we get

$$\langle\phi|\,\mathcal{S}_{J_z} + \mathcal{S}_{J^2}\,|\phi\rangle = \sum\nolimits_{j',j_z'} (e_{j',j_z'})|c_{j',j_z'}^2| \le |c_{j,j_z}|^2 \tag{10}$$

Here $|c_{j,j_z}|^2$ is the probability of projecting $|\phi\rangle$ onto the state $|j = N, j_z = N - 2K\rangle$. Our experimentally prepared mixed state ρ is a convex combination of pure states, yielding our lower bound

$$\langle\mathcal{S}_{J_z} + \mathcal{S}_{J^2}\rangle_\rho := \mathrm{Tr}[(\mathcal{S}_{J_z} + \mathcal{S}_{J^2}) \cdot \rho] \le \mathcal{F}(\rho_{j,j_z}, \rho) \tag{11}$$

4.3 Experimental Results

We construct Dicke state $|D_K^N\rangle$ circuits using the preparation scheme described in Section 4.1. To obtain the bounds on fidelity, first, we generate the untranspiled QASM circuits for Dicke State $|D_K^N\rangle$ where $2 \le N \le 10$ and $1 \le K \le N/2$. Next, we compute the bounds on the quantum fidelity using only three measurements (X, Y, and Z basis measurement). We use the formulas of Section 4.2 to estimate the lower bound $\langle\mathcal{S}_{J_z} + \mathcal{S}_{J^2}\rangle_\rho$ on quantum fidelity $\langle D_K^N|\,\rho\,|D_K^N\rangle$. We also show the probability of finding expected basis states among the total number of circuit executions (informally, called measured success probability). The definition of S_{J_z} in 8 shows that it is the measured success probability of the prepared Dicke state.

4.3.1 *Overall Results.*

Figure 3 shows the bounds for Dicke State $|D_K^N\rangle$ where the Dicke states from left to right are sorted according to the number of required CNOT gates in the untranspiled circuit. In the X axis,

[1] We note that in [20], the operator is defined as $\mathcal{S}_{J_z} = -\frac{1}{4}(J_z - j_z))^2 + 1$, which for states $|j', j_z' \neq j_z\rangle$ leads to eigenvalues ≤ 0 instead of a strict equality = 0. This results in less tight bounds; see Figure 1.

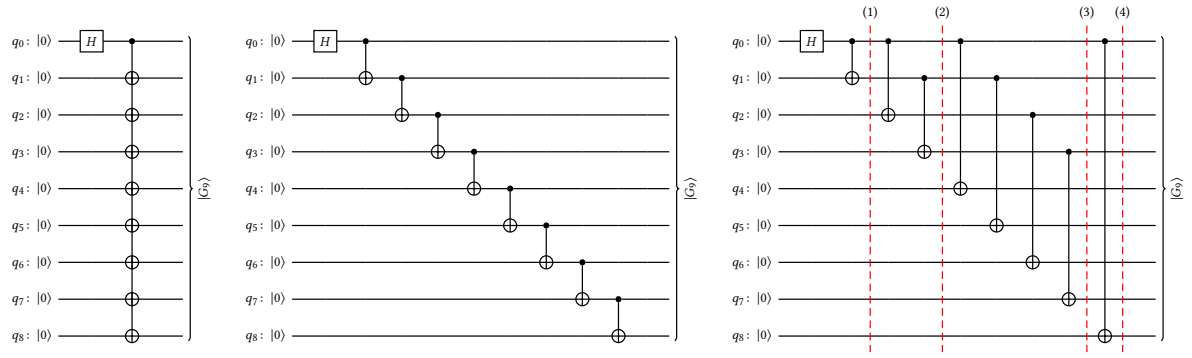

Figure 5: Preparation of a ($N = 9$)-qubit GHZ state $|G_9\rangle$: (left) Schematics, (center) Linear-depth circuit on LNN connectivity, (right) Logarithmic-depth circuit on full connectivity. For the linear depth GHZ circuit, all CNOT gates are executed consecutively and generate a linear time $O(N)$ complexity. For the logarithmic depth GHZ circuit, the gates leading to (1),(2),(3) & (4), respectively, can be executed in parallel and generate a logarithmic $O(\log N)$ complexity.

Dicke states $|D_K^N\rangle$ are represented as $D - N - K : (C)$ where N is the number of qubits, K is hamming weight and C is the number of CNOT counts. The plot shows the lower bound $\langle \mathcal{S}_{J_z} + \mathcal{S}_{J^2} \rangle_\rho$ and measurement success probability along with two-sided 68% confidence interval below and above the mean of the distribution. We observe statistical noise in the lower bound estimation for the smaller Dicke states (with few CNOTs). We also find that the fidelity lower bound decreases with the increasing number of CNOT gates on both the simulator and real hardware. Also, we observe that the lower bound estimation of Dicke states is better in hardware than in the simulator. For our largest Dicke state $|D_5^{10}\rangle$, the simulator lower bound estimation on fidelity is 0.22 while the hardware estimation is 0.46. Quantinuum specification mentions that although the simulators provide a high-fidelity representation of the hardware device's output, some variances between the results may occur as the simulation's noise models cannot fully capture the actual hardware behavior.

The sudden inconsistency of lower bound estimation from $|D_2^8\rangle$ could be because the experiments before and after $|D_2^8\rangle$ were executed in a different time span. Moreover, the experiments after $|D_3^7\rangle$ were run just after the H1-2 machine became online after calibration. The plot also shows that the measured success probability represents the upper bound of quantum fidelity, and the gap between the lower bound & the upper bound starts to increase for higher Dicke states.

4.3.2 *Number of Shots.*

We ran the Dicke state circuits on the Quantinuum H1-2E simulator using $max(150, 4 * num\_states)$ shots where $num\_states = {}^N C_K$. Figure 4 shows cumulative measurements of bounds on quantum fidelity $\langle D_K^N | \rho | D_K^N \rangle$. The left plot shows bounds on quantum fidelity for Dicke state $|D_4^8\rangle$ & the right plot shows the bounds for Dicke state $|D_4^{10}\rangle$ on H1-2 quantum device. In each plot, the X-axis shows the number of shots and the Y-axis shows the cumulative bound estimations. Each plot shows three cumulative lines: lower bound $\langle \mathcal{S}_{J_z} + \mathcal{S}_{J^2} \rangle$, upper bound measured success probability and S_{j^2}. The plots also show two-sided 68% confidence intervals below mean and above mean for lower bound and measured success probability S_{J_z}. The plots are scaled according to the maximum number of shots used in the execution of the circuit. In each plot, we find that initially, there is a lot of fluctuation in the lower and upper bound estimations, but the estimations start to get balanced with the increasing number of shots. Similarly, the confidence interval region follows the lower bound estimation and shows how the estimation starts to be stable at the end. The cumulative measurement success probability of the experiments represents the upper bound of quantum fidelity, stabilizing faster than the lower bounds.

5 FIDELITY LOWER BOUNDS FOR GHZ STATES

We provide experimental lower bound estimations on quantum fidelity for GHZ states $|G_N\rangle$ (up to $N = 20$). First, we discuss the circuit preparation strategies. Then, we provide lower bound expressions for estimating quantum fidelity in state preparation. Finally, we present experimental results for fidelity estimation in Quantinuum's H1-1 quantum processor.

5.1 State Preparation

An N-qubit GHZ state is comprised of equal weight superposition of all zeros and all ones defined as,

$$|G_N\rangle = \frac{|0\rangle^{\otimes N} + |1\rangle^{\otimes N}}{\sqrt{2}}. \tag{12}$$

The straightforward way to prepare $|G_N\rangle$ is first initializing all qubits to $|0\rangle^{\otimes N}$. The next step is adding a Hadamard gate H to the first qubit and then consecutively adding a CNOT gate between i^{th} and $(i+1)^{th}$ qubit, where $i = 0$ to $N-1$. This circuit generates a linear time complexity of N. Recent work showed that some CNOT gates could be rearranged in GHZ state preparation without affecting the output state, allowing execution of the CNOT gates in parallel [7]. Such rearrangement reduces the execution step of the GHZ circuit and generates logarithmic depth GHZ circuits with time complexity $1 + log_2 N$. Figure 5 shows $N = 10$ qubit linear (left) and logarithmic depth (right) GHZ state preparation from initial state $|0\rangle^{\otimes N}$. Both circuits contain N gates (1 Hadamard and $(N-1)$ CNOTs). The dotted lines in the right plot indicate slices within which the CNOT gates can be performed in parallel. The linear

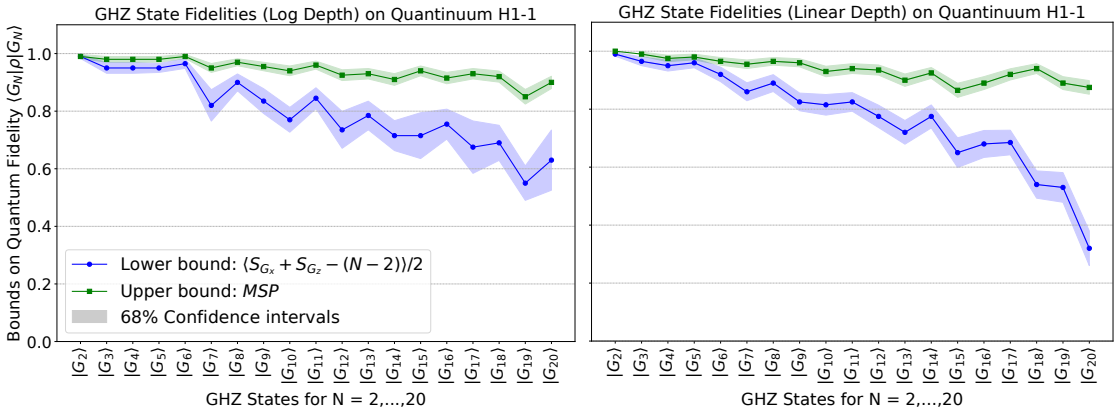

Figure 6: Upper and lower bounds on quantum fidelity $\langle G_N|\,\rho\,|G_N\rangle$ for GHZ States $|G_N\rangle$ on Quantinuum H1-1 up to $N = 20$, including 68% confidence intervals. The left plot shows results for logarithmic depth state preparation circuits, while the right plot shows results for a linear depth state preparation.

depth circuit (left) requires serial execution of the CNOT gates after the first Hadamard gate that induces linear time complexity of $N = 10$. In the logarithmic depth $|G_N\rangle$ circuit, the CNOT gates in each time slice execute in parallel generating logarithmic complexity of $1 + log_2 N = 1 + log_2(10) \approx 4$.

5.2 Lower bounds for fidelity estimation

GHZ states belong to the family of stabilizer states used in quantum error correction procedures. From [20], we find symmetry operators can define that stabilizer states,

$$\hat{O}_s = +1\,|\psi\rangle\,; s \in [1, S] \tag{13}$$

Here, the stabilizer operator $\hat{O}_s$ are products of Pauli operators that take +1 or -1 as possible eigenvalues. An stabilizer state $|\psi\rangle$ can be uniquely defined by 13 where $G_s = \{\hat{O}_1, .., \hat{O}_s\}$ forms the stabilizer group. G_s can also be defined using its L linear independent generators [10], $G_s \equiv (\hat{g_1}, ..., \hat{g_L})$ where

$$\hat{g_i}\,|\psi\rangle = +1\,|\psi\rangle\,, i\epsilon[1, L] \tag{14}$$

Thus, the state $|\psi\rangle$ can be expressed as $|\psi\rangle = |g_1 = 1, ..., g_L = 1\rangle$ while the density operator ρ_ψ can be defined as

$$\rho_\psi = |g_1{=}1, ..., g_L{=}1\rangle\,\langle g_1{=}1, ..., g_L{=}1| = \frac{1}{2^L}\prod_{i=1}^{L}(\hat{g_i} + \mathbb{1}) \tag{15}$$

The fidelity of a prepared state $|\rho\rangle$ can be measured by computing the expectations listed in 15. From [20], we find that a lower bound on the fidelity can be estimated using the operator $\mathcal{S}_{G_s} = \frac{1}{2}[(\sum_{i=1}^{L}\hat{g_i}) - (L-2)]$. When the operator $\mathcal{S}_{G_s}$ is applied to the state $|\psi\rangle = |g_1, ..., g_L\rangle$, we get,

$$\mathcal{S}_{G_s}\,|g_1, ..., g_L\rangle = e_{g_1,...,g_L}\,|g_1, ..., g_L\rangle\,, (g_i = \pm 1) \tag{16}$$

where $e_{1,...,1} = 1$ and $e_{g_1,...g_L \leq 0}$. The lower bound on fidelity between prepared state ρ and expected state $|G_N\rangle$ becomes

$$\mathcal{F}(|G_N\rangle\,, \rho) \geq \langle \mathcal{S}_{G_s}\rangle_\rho \tag{17}$$

Using the formulas above for an N-qubit GHZ state $|G_N\rangle$, the stabilizer group can be defined as $G_s \equiv (\sigma_x^1\sigma_x^2..\sigma_x^N, \sigma_z^1\sigma_z^2, \sigma_z^2\sigma_z^3, ..., \sigma_z^{N-1}\sigma_z^N)$.

We can estimate the lower bounds on GHZ state fidelities using only the Pauli X and Z measurements and $\mathcal{S}_{G_s}$ will be defined as

$$\mathcal{S}_{G_s} = \frac{1}{2}[\mathcal{S}_{G_x} + \mathcal{S}_{G_z} - (N-2)] \tag{18}$$

where $\mathcal{S}_{G_x}$ represents product of Pauli X operator on $i = 1$ to N qubits and $\mathcal{S}_{G_z}$ represents sum of the pairwise products of Pauli Z operator on i^{th} and $(i+1)^{th}$ qubit upto N^{th} qubit. For a 4-qubit GHZ state, we get $N = 4$ and $L = 4$,

$$\mathcal{S}_{G_s} = \frac{1}{2}[\sigma_x^1\sigma_x^2\sigma_x^3\sigma_x^4 + \sigma_z^1\sigma_z^2 + \sigma_z^2\sigma_z^3 + \sigma_z^3\sigma_z^4 - 2]. \tag{19}$$

Basically, we need to compute the expectation of the product of Pauli X measurement on each of the four qubits by taking +1 for even parity and -1 for odd parity. Similarly, we compute the consecutive pairwise product of Pauli Z measurement on qubits 1 & 2, 2 & 3, and 3 & 4 by checking the pairwise parity. Then, we estimate the fidelity lower bound for the GHZ state by taking the average of those products and subtracting $N - 2$ from the sum.

5.3 Experimental Results

We prepare linear depth and logarithmic depth GHZ states $|G_N\rangle$ circuits mentioned in Section 5.1. In this experiment, we generate untranspiled QASM circuits for GHZ states $|G_N\rangle$, where $2 \leq N \leq 20$. We compute the bounds on quantum fidelity using only two measurements (X and Z basis measurement) instead of measuring 3^N state tomography circuits to measure the closeness of prepared GHZ state ρ to the expected state $|G_N\rangle$. To estimate lower bound $\langle \mathcal{S}_{G_s}\rangle_\rho$, we followed the idea described in Section 5.2.

5.3.1 *Overall Results.*

Figure 6 shows the bounds for GHZ state $|G_N\rangle$. The GHZ states are sorted left to right according to CNOT gate counts in untranspiled GHZ circuits. The left plot shows bounds for logarithmic depth GHZ state circuits, while the right plot shows bounds for the linear depth GHZ circuits. Both plots show a lower bound on quantum fidelity and measurement success probability along with a 68% confidence interval below and above the mean of the distribution. For both log and linear depth circuits, the lower bound on

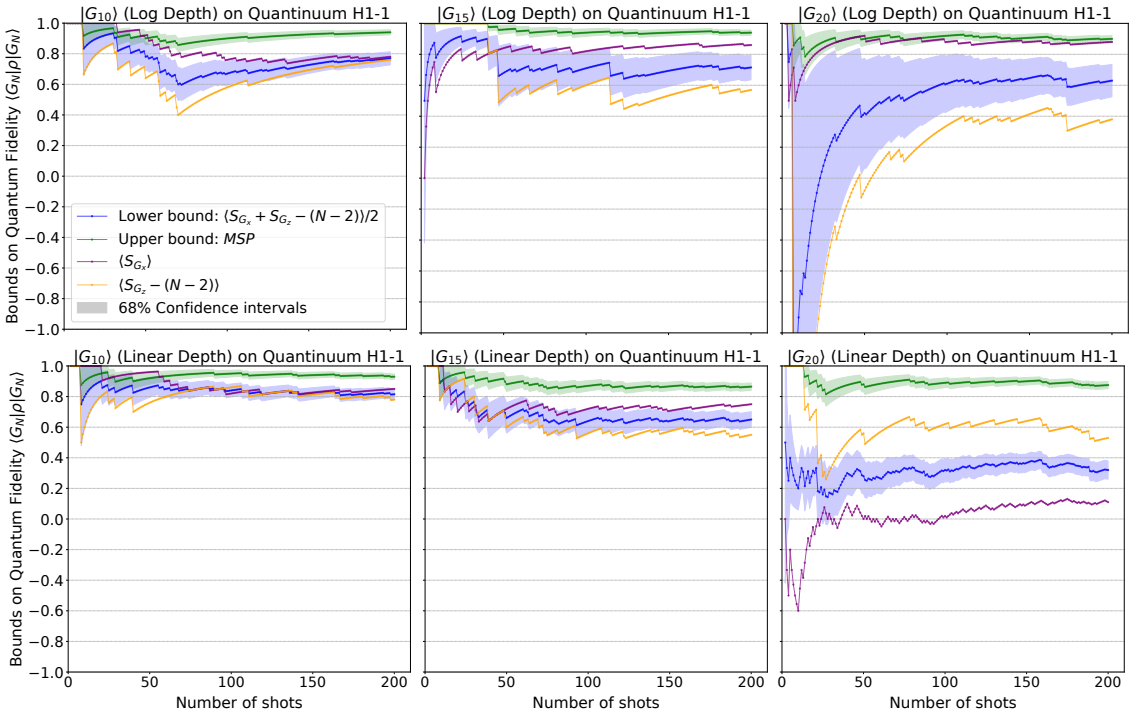

Figure 7: Evolving bounds on quantum fidelity $\langle G_N|\,\rho\,|G_N\rangle$ for GHZ States *(left)* $|G_{10}\rangle$, *(center)* $|G_{15}\rangle$ & *(right)* $|G_{20}\rangle$ on Quantinuum H1-1 over 200 shots. *(top row)* Plots show bounds for logarithmic depth GHZ state preparation circuits; *(bottom row)* plots show bounds for linear depth GHZ state preparation. Each plot shows the cumulative progress of lower bound estimation, including confidence intervals. All experiments were run back to back in batch mode.

fidelity decreases almost linearly, albeit with few variations with increasing CNOT counts for higher N. The gap between the lower bound and measured success probability increases with increasing CNOT count. The linear circuit shows a faster drop for higher GHZ states than the log depth circuit, which is expected as logarithmic depth circuits require fewer time steps for circuit execution. In both plots, we observe a few irregular ups and downs in the lower bound estimation, which could be because of the statistical noise. The gap between the lower bound and confidence interval region stays almost close in all GHZ states. Our investigation finds that expectation $\mathcal{S}_{G_s}$ (defined as the product of Pauli X operations on each qubit) starts to drop from $|G_{11}\rangle$ and becomes more significant from $|G_{17}\rangle$. There are two flat decreases from linear depth GHZ state $|G_{17}\rangle$ to $|G_{18}\rangle$ and $|G_{19}\rangle$ to $|G_{20}\rangle$, which could be caused by the qubit rearrangement in Quantinuum H1-1 device.

5.3.2 *Number of Shots.*

To see the effect of the number of shots on the quantum fidelity of GHZ states, we execute the GHZ states $|G_N\rangle$ where $2 \leq N \leq 20$ for 200 shots on the H1-1 quantum processor. We estimate the cumulative lower bound distribution on quantum fidelity $\langle G_N|\,\rho\,|G_N\rangle$ from initial to up to i^{th} shot where $i = 2$ to 200. Figure 7 shows the estimations of bounds on quantum fidelity $\langle G_N|\,\rho\,|G_N\rangle$ for GHZ states on Quantinuum H1-1 quantum processor. The upper two plots (left and right) show logarithmic depth $|G_{10}\rangle$, $|G_{15}\rangle$ & $|G_{20}\rangle$ states, and the bottom two plots (left and right) show linear depth $|G_{10}\rangle$, $|G_{15}\rangle$ & $|G_{20}\rangle$ states. Each plot shows lower bound estimation, measured success probability, and expectations of Pauli X & Z measurements for GHZ state $|G_N\rangle$ preparation. The plots also include a 68% confidence interval region below and above the mean of the lower bound and measured success probability. In each plot, the cumulative measurements start with a lot of fluctuations that become balanced with increasing the number of shots. We observe that all the measurements are more steady in the $|G_{10}\rangle$ plot for both linear and logarithmic depth circuits than $|G_{15}\rangle$ and $|G_{20}\rangle$ plots. We find that the expectation $\mathcal{S}_{\mathcal{G}_\S}$ (purple line) drops significantly for $|G_{20}\rangle$. It could be possible that larger GHZ states require more shots to become stable. Additionally, we observe that the confidence interval region for the log depth $|G_{20}\rangle$ circuit is less stable than the linear depth circuit. Besides, the upper bound measured success probability stays almost stable in linear and log depth circuits.

6 CONCLUSION

We have demonstrated good fidelity values for the Dicke and GHZ, highly entangled quantum states, prepared on Quantinuum H1 ion trap systems. Since direct fidelity estimation through full-state tomography does not scale, we compute lower bounds on the fidelity with exponentially reduced overhead for those states. For the first time and after 15 years of its theoretical introduction, we show that these bounds are tight enough for meaningful fidelity estimations on the newest NISQ devices. We give state preparation fidelity lower bounds of 0.46 for the Dicke State $|D_5^{10}\rangle$ and 0.73 for the GHZ State $|G_{20}\rangle$ which match or exceed exact fidelity records recently

achieved on superconducting systems for the much smaller states $|D_3^6\rangle$ and $|G_5\rangle$, respectively. This improved performance is due to improvements in NISQ hardware and efficient implementations of the latest circuits.

7 ACKNOWLEDEMENT

The authors would like to thank the anonymous reviewers.

REFERENCES

[1] 2021. Qiskit: An Open-source Framework for Quantum Computing. https://doi.org/10.5281/zenodo.2573505

[2] 2021. Quantinuum H1, Powered by Honeywell. http://groups.csail.mit.edu/

[3] Shamminuj Aktar, Andreas Bärtschi, Abdel-Hameed A Badawy, and Stephan Eidenbenz. 2022. A Divide-and-Conquer Approach to Dicke State Preparation. *IEEE Transactions on Quantum Engineering* 3 (2022), 1–16. https://doi.org/10.1109/TQE.2022.3174547 arXiv:2112.12435

[4] Andreas Bärtschi and Stephan Eidenbenz. 2019. Deterministic Preparation of Dicke States. In *22nd International Symposium on Fundamentals of Computation Theory, FCT'19*. 126–139. https://doi.org/10.1007/978-3-030-25027-0_9 arXiv:1904.07358

[5] Andreas Bärtschi and Stephan Eidenbenz. 2022. Short-Depth Circuits for Dicke State Preparation. In *IEEE International Conference on Quantum Computing & Engineering QCE'22*. arXiv:2207.09998 To appear..

[6] Andrew W Cross, Lev S Bishop, John A Smolin, and Jay M Gambetta. 2017. Open quantum assembly language. *arXiv preprint* (2017). arXiv:1707.03429

[7] Cruz, Diogo and Fournier, Romain and Gremion, Fabien and Jeannerot, Alix and Komagata, Kenichi and Tosic, Tara and Thiesbrummel, Jarla and Chan, Chun Lam and Macris, Nicolas and Dupertuis, Marc-André and Javerzac-Galy, Clément. 2019. Efficient Quantum Algorithms for GHZ and W States, and Implementation on the IBM Quantum Computer. *Advanced Quantum Technologies* 2, 5-6 (2019), 1900015. https://doi.org/10.1002/qute.201900015 arXiv:1807.05572

[8] Andreas Elben, Steven T Flammia, Hsin-Yuan Huang, Richard Kueng, John Preskill, Benoît Vermersch, and Peter Zoller. 2022. The randomized measurement toolbox. *arXiv preprint* (2022). arXiv:2203.11374

[9] Steven T Flammia and Yi-Kai Liu. 2011. Direct fidelity estimation from few Pauli measurements. *Physical Review Letters* 106, 23 (2011), 230501. https://doi.org/10.1103/PhysRevLett.106.230501 arXiv:1104.4695

[10] Daniel Gottesman. 1997. *Stabilizer codes and quantum error correction. Caltech Ph. D.* Ph. D. Dissertation. Thesis, eprint. arXiv:quant-ph/9705052

[11] Otfried Gühne, Chao-Yang Lu, Wei-Bo Gao, and Jian-Wei Pan. 2007. Toolbox for entanglement detection and fidelity estimation. *Physical Review A* 76, 3 (2007), 030305. https://doi.org/10.1103/PhysRevA.76.030305 arXiv:0706.2432

[12] Xinhe Jiang, Kun Wang, Kaiyi Qian, Zhaozhong Chen, Zhiyu Chen, Liangliang Lu, Lijun Xia, Fangmin Song, Shining Zhu, and Xiaosong Ma. 2020. Towards the standardization of quantum state verification using optimal strategies. *npj Quantum Information* 6, 1 (2020), 1–8. https://doi.org/10.1038/s41534-020-00317-7 arXiv:2002.00640

[13] Richard Jozsa. 1994. Fidelity for mixed quantum states. *Journal of Modern Optics* 41, 12 (1994), 2315–2323.

[14] Zihao Li, Yun-Guang Han, and Huangjun Zhu. 2019. Efficient verification of bipartite pure states. *Physical Review A* 100, 3 (2019), 032316. https://doi.org/10.1103/PhysRevA.100.032316 arXiv:1901.09783

[15] Zihao Li, Yun-Guang Han, and Huangjun Zhu. 2020. Optimal verification of greenberger-horne-zeilinger states. *Physical Review Applied* 13, 5 (2020), 054002. https://doi.org/10.1103/PhysRevApplied.13.054002 arXiv:1909.08979

[16] Ye-Chao Liu, Xiao-Dong Yu, Jiangwei Shang, Huangjun Zhu, and Xiangdong Zhang. 2019. Efficient verification of Dicke states. *Physical Review Applied* 12, 4 (2019), 044020. https://doi.org/10.1103/PhysRevApplied.12.044020 arXiv:1904.01979

[17] Chandra Sekhar Mukherjee, Subhamoy Maitra, Vineet Gaurav, and Dibyendu Roy. 2020. Preparing Dicke States on a Quantum Computer. *IEEE Transactions on Quantum Engineering* 1 (2020), 1–17. https://doi.org/10.1109/TQE.2020.3041479

[18] Michael A. Nielsen and Isaac L. Chuang. 2000. *Quantum Computation and Quantum Information*. Cambridge University Press.

[19] Sam Pallister, Noah Linden, and Ashley Montanaro. 2018. Optimal verification of entangled states with local measurements. *Physical Review Letters* 120, 17 (2018), 170502. https://doi.org/10.1103/PhysRevLett.120.170502 arXiv:1709.03353

[20] Rolando D Somma, John Chiaverini, and Dana J Berkeland. 2006. Lower bounds for the fidelity of entangled-state preparation. *Physical Review A* 74, 5 (2006), 052302. https://doi.org/10.1103/PhysRevA.74.052302 arXiv:quant-ph/0606023

[21] Yuuki Tokunaga, Takashi Yamamoto, Masato Koashi, and Nobuyuki Imoto. 2006. Fidelity estimation and entanglement verification for experimentally produced four-qubit cluster states. *Physical Review A* 74, 2 (2006), 020301. https://doi.org/10.1103/PhysRevA.74.020301

[22] Kun Wang and Masahito Hayashi. 2019. Optimal verification of two-qubit pure states. *Physical Review A* 100, 3 (2019), 032315. https://doi.org/10.1103/PhysRevA.100.032315 arXiv:1901.09467

[23] Xiao-Dong Yu, Jiangwei Shang, and Otfried Gühne. 2019. Optimal verification of general bipartite pure states. *npj Quantum Information* 5, 1 (2019), 1–5. https://doi.org/10.1038/s41534-019-0226-z arXiv:1901.09856

[24] Wen-Hao Zhang, Chao Zhang, Zhe Chen, Xing-Xiang Peng, Xiao-Ye Xu, Peng Yin, Shang Yu, Xiang-Jun Ye, Yong-Jian Han, Jin-Shi Xu, et al. 2020. Experimental optimal verification of entangled states using local measurements. *Physical Review Letters* 125, 3 (2020), 030506. https://doi.org/10.1103/PhysRevLett.125.030506 arXiv:1905.12175

[25] Xiaoqian Zhang, Maolin Luo, Zhaodi Wen, Qin Feng, Shengshi Pang, Weiqi Luo, and Xiaoqi Zhou. 2021. Direct fidelity estimation of quantum states using machine learning. *Physical Review Letters* 127, 13 (2021), 130503. https://doi.org/10.1103/PhysRevLett.127.130503 arXiv:2102.02369

[26] Huangjun Zhu and Masahito Hayashi. 2019. Efficient verification of hypergraph states. *Physical Review Applied* 12, 5 (2019), 054047. https://doi.org/10.1103/PhysRevApplied.12.054047 arXiv:1806.05565

[27] Huangjun Zhu and Masahito Hayashi. 2019. Efficient verification of pure quantum states in the adversarial scenario. *Physical Review Letters* 123, 26 (2019), 260504. https://doi.org/10.1038/s41534-021-00455-6 arXiv:1909.01900

[28] Huangjun Zhu and Masahito Hayashi. 2019. General framework for verifying pure quantum states in the adversarial scenario. *Physical Review A* 100, 6 (2019), 062335. https://doi.org/10.1103/PhysRevA.100.062335 arXiv:1909.01943

[29] Huangjun Zhu and Masahito Hayashi. 2019. Optimal verification and fidelity estimation of maximally entangled states. *Physical Review A* 99, 5 (2019), 052346. https://doi.org/10.1103/PhysRevA.99.052346 arXiv:1901.09772